Colloids and Surfaces B: Biointerfaces 121 (2014) 400–408

Contents lists available at ScienceDirect

Colloids and Surfaces B: Biointerfaces

journal homepage: www.elsevier.com/locate/colsurfb

# Biosensor utilizing a liquid crystal/water interface functionalized with poly(4-cyanobiphenyl-4′-oxyundecylacrylate-*b*-((2-dimethyl amino) ethyl methacrylate))

Muhammad Omer[a], Mashooq Khan[a], Young Kyoo Kim[a], Joon Hyung Lee[b], Inn-Kyu Kang[a], Soo-Young Park[a,*]

[a] School of Applied Chemical Engineering, Kyungpook National University, Daegu 702-701, Republic of Korea
[b] School of Advanced Materials Engineering, Kyungpook National University, Daegu 702-701, Republic of Korea

ARTICLE INFO

*Article history:*
Received 1 February 2014
Received in revised form 15 May 2014
Accepted 11 June 2014
Available online 25 June 2014

*Keywords:*
Weak cationic polyelectrolyte
Poly(4-cyanobiphenyl-4′-oxyundecylacrylate-*b*-((2-dimethyl amino) ethyl methacrylate))
Protein
Langmuir Blodgett films
DNA
Biosensor

ABSTRACT

The interface between the nematic liquid crystal, 4-cyano-4′-pentylbiphenyl (5CB) and water within a transmission electron microscopy (TEM) grid cell coated with the pH-dependent weak cationic amphiphilic block copolymer poly((4-cyanobiphenyl-4′-oxyundecylacrylate)-*b*-((2-dimethyl amino) ethyl methacrylate)) (LCP-*b*-PDMAEMA) (which was successfully synthesized by reversible addition-fragmentation chain transfer (RAFT) polymerization) was subsequently evaluated for protein and deoxyribonucleic acid (DNA) detection. The LCP-*b*-PDMAEMA monolayer was fabricated using a Langmuir Blodgett trough, transferred to the 5CB-filled TEM grid, and placed on the octadecyltrichlorosilane-coated glass ($TEM_{PDMAEMA}$) in such a way that the LCP chains were immersed in the 5CB while the PDMAEMA chains were pointed away from the 5CB surface and immersed in water. Several model proteins such as bovine serum albumin (BSA), hemoglobin (Hb), and chymotrypsinogen (ChTg) were tested at pH values ranging from 2 to 12 to determine the role of the charge state of the protein on protein detection by a weak polyelectrolyte such as PDMAEMA. PDMAEMA contains cationic and neutral states below and above the pKa value, respectively, and is thus able to absorb proteins below its pKa threshold through electrostatic interactions. BSA exhibited a homeotropic to planar (H–P) change in orientation within the $TEM_{PDMAEMA}$ grid cell at concentrations greater than 0.02 wt% within the pH range between the isoelectric point (pI) of BSA and the pKa of PDMAEMA, where the charge states of BSA and PDMAEMA were negative and positive, respectively. However, this change in orientation did not occur with other proteins that exhibited a pI higher than the pKa of PDMAEMA due to the electrostatic repulsions resulting from their same cationic charges. This result indicates that the electrostatic interactions between proteins and PDMAEMA are a major contributing factor for protein detection by the H–P transformation within the $TEM_{PDMAEMA}$ grid cell. DNA, a pH-independent strong anionic polyelectrolyte, was also tested with the $TEM_{PDMAEMA}$ grid cell, and it exhibited an H–P transformation at the charged state of PDMAEMA below its pKa threshold at concentrations higher than 0.01 wt%. Thus, we demonstrated that the $TEM_{PDMAEMA}$ grid cell effectively facilitated the detection of negatively charged biomaterials (i.e.; protein and DNA) through the H–P transformation using the polarized optical microscope. This simple and inexpensive experimental set-up for non-specific biomaterial detection lays the basic groundwork for developing effective biosensors using polyelectrolytes.



## 1. Introduction

The scientific community has shown considerable interest in the synthesis of block copolymers over the past decade due to their various applications in both academic and industrial settings. Monomers bearing specific properties are often incorporated into block copolymers to tailor their end applications. Block copolymers containing a polyelectrolyte block carrying ionizable groups with electrostatic charges have been widely studied and incorporated into sensors [1–4]. In polar solvents (e.g., water) these ionizable groups can dissociate into charged groups on the polymer chains while releasing counter ions into the solution. Polyelectrolytes can

* Corresponding author. Tel.: +82 53 950 5630; fax: +82 53 950 6623.
*E-mail address:* psy@knu.ac.kr (S.-Y. Park).

http://dx.doi.org/10.1016/j.colsurfb.2014.06.028
0927-7765/

be classified into strong or weak polyelectrolytes according to the nature of the ionic groups. A strong polyelectrolyte is in the ionized state regardless of the pH of the solution, while the ionized state of a weak polyelectrolyte is dependent on the pH of the solution. A weak anionic polyelectrolyte is deprotonated to the anionic state when the pH of the solution is higher than the pKa of the polyelectrolyte, and a weak cationic polyelectrolyte is protonated to the cationic state when the pH of the solution is lower than the pKa of the polyelectrolyte. The conformation of the polyelectrolyte primarily depends on the electrostatic interactions between the charged groups of the polyelectrolyte. Highly charged polyelectrolytes lead to an increase in osmotic pressure, which causes the chains to adopt an expanded, rigid, rod-like conformation [5–9]. Therefore, the pH of the solution also controls the chain conformation through protonation (or deprotonation) of weak polyelectrolytes.

Polyelectrolytes have always been crucial for sensors which are designed to detect electrostatically charged analytes such as toxic inorganic ions [10–12], proteins [2,3], or deoxyribonucleic acid (DNA) [13]. Previous reports confirm that block copolymers in which a polyelectrolyte block is covalently bonded to a non-polyelectrolyte block may exhibit other useful properties in addition to self-assembly at the nanoscale in bulk and in solution. For example, an ordered nanoporous membrane comprising QP4VP-*b*-PS (where QP4VP and PS refer to quaternized poly(4-vinylpyridine) and polystyrene, respectively) has been utilized in the separation of similarly sized proteins [14], while a composite material comprising carbon nanotubes containing the weak polyelectrolyte poly(2-hydroxyethyl methacrylate)-*b*-poly(2-(dimethylamino)ethyl methacrylate) (PHEMA-*b*-PDMAEMA) has been utilized in the immobilization of hemoglobin for the fabrication of electrochemical biosensors [3]. For protein biosensors, either labeled-probe or label-free strategies have been employed in the generation of signals. The former strategy involves labeling the analytes with species such as radioisotopes or fluorescent dyes [15], while the latter strategy relies on the inherent properties of the analyte that are directly measurable, such as the mass or dielectric properties [16]. Analytical methods such as Fourier transform infrared (FT-IR) spectroscopy [17], fluorimetry [18], and high-performance liquid chromatography (HPLC) [18,19] have been previously utilized for the detection of proteins. While these methods are typically quite accurate, they often require complex procedures for sample preparation. Thus, the rapid and reliable detection of proteins is still a challenge that has yet to be addressed.

Biosensors based on liquid crystal (LC) are rapid and effective detection tools that utilize a label-free strategy and have subsequently attracted much attention in recent years [20–27]. Because of their high sensitivity and rapid response with respect to orientation, small-molecule LCs are an attractive medium for detecting chemical/biochemical events occurring at an interface as a result of optical changes that can be viewed with the aid of a polarized optical microscopy [28–31]. An optical change can occur as a result of a change in orientation of the LCs from vertical to parallel alignments at the water/LC interface upon adsorption of biomaterials [32]. The vertical and parallel alignments are referred to as homeotropic and planar orientations, respectively. LC-based biosensor systems typically employ small receptor molecules mixed with the LCs. However, upon mixing the polyelectrolyte with small LC molecules, phase separation occurs due to the thermodynamic incompatibility between the two compounds. However, this phenomenon could be overcome by the block copolymerization of the polyelectrolyte with another block that is more compatible with the small LC molecules. The most compatible block may be a liquid crystal polymer (LCP) that possesses the same mesogenic groups in the side chains with LC molecules. Since the polyelectrolyte-*b*-LCP can lead to micelle formation in the selected solvent (e.g. water), a facile strategy for incorporating the block copolymer into the LC molecules is to transfer the block copolymer monolayer, which was produced using a Langmuir Blodget (LB) trough, to the LC surface [33]. This method has advantages over the existing method of mixing receptor molecules with small LC molecules because the properties of monolayer can be easily controlled by adjusting the density of the receptor macromolecules per unit area [24].

In this report, an amphiphilic diblock copolymer, poly(4-cyanobiphenyl-4′-oxyundecylacrylate-*b*-((2-dimethyl amino) ethyl methacrylate)) (LCP-*b*-PDMAEMA) was synthesized through reversible addition fragmentation chain transfer (RAFT) polymerization where LCP is compatible with the used LC molecules, 4-cyano-4′-pentylbiphenyl (5CB, nematic at room temperature) and PDMAEMA is a weak cationic polyelectrolyte. The LCP and PDMAEMA blocks of the block copolymer function as a transducer and a bio-receptor, respectively, at the LC/water interface by transferring this monolayer onto the 5CB of the TEM grid. The TEM grid cell was then evaluated for protein and DNA detection at various pH values and solution concentrations to determine the sensitivity and the possible detectable pH range for the homeotropic to planar (H–P) change in orientation.

## 2. Experimental

### 2.1. Materials

The DMAEMA monomer (Sigma–Aldrich) was purified by passing through an alumina column to remove any inhibitor present in the sample, while azobis(isobutyronitrile) (AIBN, Junsei) was recrystallized from methanol. 5CB, hexane, octadecyltrichlorosilane (OTS), phenylmagnesium bromide, tetrahydrofuran (THF), 4-cyano-4′-hydroxybiphenyl, 11-bromo-1-undecanol, methanol, potassium hydroxide, acryloyl chloride, triethylamine, carbon disulfide, methyl α-bromophenylacetate, hexane/diethyl ether, anhydrous magnesium sulfate, DNA, bovine serum albumin (BSA), hemoglobin (Hb), and chymotrypsinogen (ChTg) were purchased from Sigma–Aldrich at the highest available purity and used as received. All water used in this study was purified using a Millipore Milli-Q system and the resistivity was less than 16 MΩ cm. pH buffer solutions were purchased from Samchun© (Korea) and used as received. Copper specimen grids (G75, with a grid hole width of 285 μm, a pitch of 340 μm, a bar width of 55 μm, and a rim width of 0.225 mm) were supplied by Gilder Grids (United Kingdom).

### 2.2. Synthesis of the chain transfer agent and the LC monomer

The chain transfer agent (CTA) S-methoxycarbonylphenylmethyl dithiobenzoate (MCPDB) was prepared by following the procedure developed by Perrier et al. [34,35], and the overall scheme is detailed in Supplementary Information (SI) Scheme 1. A solution of phenylmagnesium bromide (3.49 mL) in THF (28 mL) was heated to 50 °C and carbon disulfide (1.58 mL, 26.0 mmol) was added to the solution dropwise over approximately 20 min to produce a dark brown solution. Methyl α-bromophenylacetate (1.37 mL, 8.7 mmol) was then added to the solution, and the reaction temperature was raised to 80 °C and maintained for 13 h. Ice water (∼100 mL) was then added to the solution to immediately terminate the reaction and remove any water-soluble byproducts. The solution was then transferred to a separating funnel and diethyl ether (∼100 mL) was added to the solution. The solution was shaken and then separated into two immiscible layers consisting of aqueous (containing THF) and diethyl ether solutions after 20 min. The diethyl ether solution was subsequently extracted from separating funnel. The combined organic extracts were then rinsed with water and dried over anhydrous magnesium sulfate. After the

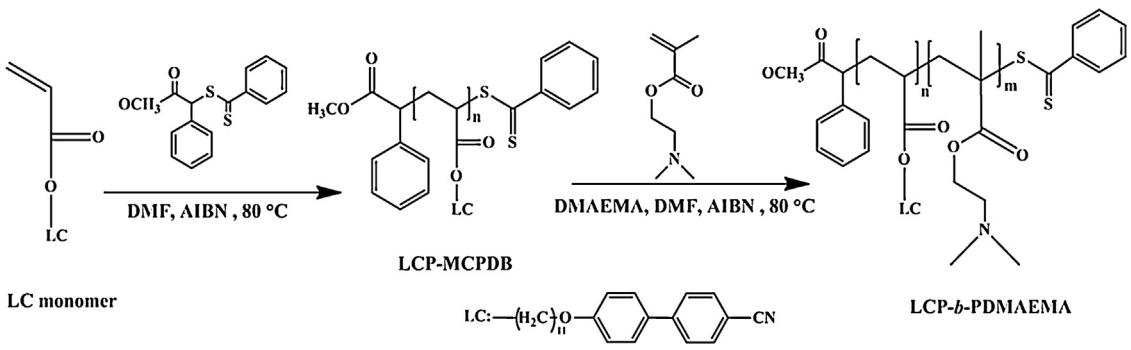


**Scheme 1.** Synthesis of LCP-*b*-PDMAEMA through RAFT polymerization.

solvent was removed, column chromatography was performed using a dichloromethane and *n*-hexane mixture (2/1, v/v) to produce an orange red oil (52.4%).

An LC monomer, LC11, was prepared following a previously reported procedure [36,37]. LC11 monomers were synthesized through the etherification of 4-cyano-4′-hydroxybiphenyl (4.02 g, 20.62 mmol) and 11-bromo-1-undecanol (5.23 g, 20.80 mmol). 11-Bromo-1-undecanol was added dropwise to a solution of 4-cyano-4′-hydroxybiphenyl and potassium hydroxide (1.38 g, 24.67 mmol) in methanol (40.01 mL), and the mixture solution was then heated under reflux for 25 h. After refluxing, the product was recrystallized twice from methanol (yield 65%) and subsequently treated with acryloyl chloride (0.23 g, 2.45 mmol) and triethylamine (0.40 mL, 2.84 mmol) to yield a mesogenic monomer as can be seen in Scheme SI 2. After being stirred for 16 h at room temperature, the LC11 was purified by recrystallizing twice from methanol (yield 45%) [35]. Figs. SI 1 and SI 2 display the NMR spectra of MCPDB and LC11, respectively. Every peak could be assigned to the protons of both compounds with respect to position and integrated area; the detailed assignment information is provided in the figure captions.

### 2.3. Synthesis of macroinitiator

The macroinitiator, MCPDB-terminated poly(4-cyanobiphenyl-4′-oxyundecylacrylate) (LCP-MCPDB) was synthesized through RAFT polymerization. LC11 (419.25 mg, 1 mmol), MCPDB (CTA) (12.68 mg, 0.042 mmol), and DMF (1.54 mL) were added to a graduated vial and dry nitrogen for bubbled through the solution for 60 min. AIBN (1.72 mg, 0.011 mmol) was placed in a Schlenk flask and stored under vacuum for 60 min. The solution containing LC11 and MCPDB was then introduced into the flask containing AIBN using a syringe needle, which was previously purged with nitrogen. The flask was placed in an oil bath at 80 °C for 16 h to initiate the RAFT reaction. LCP-MCPDB was then precipitated from a water and methanol mixture (1/1, v/v). The number average molecular weight ($M_n$) and polydispersity index (PDI) of the homopolymer were 4.40K and 1.1, respectively. Volatile materials were removed using a vacuum oven at 40 °C to yield the dry LCP-MCPDB homopolymer. The polymerization scheme for the synthesis of LCP-MCPDB is shown in Scheme 1. Fig. 2 displays the $^1$H NMR data of LCP-MCPDB including the assignment of the protons.

### 2.4. Synthesis of the block copolymer

For the synthesis of poly(4-cyanobiphenyl-4′-oxyundecylacrylate-*b*-((2-dimethyl amino) ethyl methacrylate)) (LCP-*b*-PDMAEMA), AIBN (1.576 mg, 0.0096 mmol), DMAEMA (0.674 mL, 4.00 mmol), LCP-MCPDB (70.400 mg, 0.016 mmol), and DMF (3.688 mL) were added to a Schlenk flask and degassed using three freeze–thaw evacuation cycles. The flask was then placed in an oil bath at 80 °C for 24 h under a nitrogen atmosphere. The synthesized block copolymers were precipitated from *n*-hexane three times and the volatile materials were removed under vacuum to produce a dry sample of the block copolymer (see Scheme 1). $M_n$ and $M_w/M_n$ (PDI) were $11.06 \times 10^3$ and 1.22, respectively for the block copolymer.

### 2.5. Preparation of the TEM grid cell and the flow chamber

The TEM grid cell and the flow chamber used in this study was prepared by the same procedure as reported elsewhere [37]. Fig. SI 3 shows the schematic of the preparation of the flow chamber. The glass slides were first cleaned using piranha solution ($H_2SO_4$ and $H_2O_2$ mixture (70/30, v/v)), which reacts violently with organic materials and should therefore be handled with extreme care and stored in closed containers. The glass slides were heated for 30 min at 80 °C in the piranha solution and then rinsed sequentially with water, ethanol, and methanol, dried under nitrogen, immersed in an OTS solution in toluene (25 μl/50 mL) at 40 °C for 30 min, rinsed with methylene chloride, and finally dried under nitrogen. The OTS coating was performed for the vertical alignment of the 5CB mesogens on the glass substrate. Copper specimen grids (sequentially washed with methylene chloride, ethanol, and methanol) were placed on the surface of the small OTS-coated glass which had previously been glued onto a second glass slide with epoxy (Fig. SI 3a). A small amount of 5CB (~1 μL) was dispensed onto each grid by dropping and the excess 5CB was removed by bringing a narrow capillary tube into contact with the TEM grid. The thickness of the 5CB layer on the TEM grid was approximately 18 μm. LCP-*b*-PDMAEMA (1.0 wt%) was dissolved in THF/water mixture (1/1, v/v) to form the LB monolayer. An LCP-*b*-PDMAEMA solution (0.1 mL) was then spread on the water in the LB bath to prepare the monolayer, and the surface pressure of the monolayer was controlled at 60 mN/m using a LB trough to obtain a constant brush density. After successful monolayer formation on the water surface (Fig. SI 4), the prepared TEM grid cell, which was previously mounted onto a silicon rubber attached to another glass slide (already placed in the LB bath [Fig. SI 3b]), was slowly inserted (TEM grid-side down) into the LB bath. The two glass slides, which were separated by the silicon rubber, were then clipped with binding clips. Inlet and outlet ports for the exchange of solvents were made by hypodermic needles pierced through silicon spacer (Fig. SI 3c).

### 2.6. Characterization

FT-IR spectroscopy was performed using a Jasco FT/IR-620 (Japan) FT-IR spectrometer with KBr pellets with a resolution of 4 $cm^{-1}$. FT-IR samples were vacuum-dried in an oven at 40 °C to remove all moisture. A small amount of the sample was mixed

with the KBr salt, ground well to produce a homogenous mixture, and then pressed into an FT-IR pellet. The molar masses and molar mass distributions were determined using gel permeation chromatography (GPC) with a PLgel Organic GPC column and an RI750F refractive index detector (Young Lin Instrument Co., Acme 9000, Korea). THF was used as an eluent at a flow rate of 0.7 mL $min^{-1}$ and the calibration was carried out using polystyrene standards (Sigma–Aldrich, USA). $^1$H NMR spectra were measured at ambient temperature with a 400 MHz Bruker spectrometer (Germany) using deuterated chloroform ($CDCl_3$) as a solvent for LCP-MCPDB and LCP-*b*-PDMAEMA. The optical photographs were obtained using a polarized optical microscope (Samwon, LSP-13, Korea) equipped with crossed polarizers and fluorescent images were observed using fluorescent microscopy (Nikon Eclipse, E600POL, Japan).

## 3. Results and discussion

### 3.1. Synthesis of LCP-b-PDMEMA

Fig. SI 5 displays the GPC traces of the synthesized LCP-MCPDB and LCP-*b*-PDMAEMA. An increase in the molecular weight of LCP-*b*-PDMEMA relative to that of LCP-MCPDB can be clearly observed. The molecular weight of LCP-*b*-PDMAEMA was LCP (4.4K)-*b*-PDMAEMA (6.7K) with a PDI of 1.22. Fig. 1a displays the $^1$H NMR spectra of LCP-MCPDB and LCP-*b*-PDMAEMA. The characteristic NMR peaks for both LCP and PDMAEMA blocks are present in the $^1$H NMR spectrum of LCP-*b*-PDMAEMA, indicating successful block copolymerization. The proton peak positions, respective integrated area, and number of protons for LCP-*b*-PDMAEMA are: $\delta$ = 0.74–0.9 (m, 6H, N–$(CH_3)_2$), 0.93–1.03 (s, 3H, $CH_3$), 1.16–1.26 (m, 14H, $(CH_2)_7$), 1.31–1.44 (m, 2H, $CH_2$), 1.69–1.79 (m, 2H, $CH_2$), 1.80–1.89 (d, 2H, $CH_2$), 2.06–2.13 (d, 1H, CH), 2.20–2.33 (m, 2H, $CH_2$), 2.47–2.63 (t, 2H, N–$CH_2$), 3.87–4.10 (t, 6H, $OCH_2$), 6.83–6.96 (d, 2H, O-ar), 7.39–7.50 (d, 2H, aromatic), and 7.52–7.68 (d, 4H, aromatic). The peak at *x* represents the protons of $H_2O$. Fig. 1b displays FT-IR spectra of LCP-MCPDB and LCP-*b*-PDMAEMA. The FT-IR spectrum of LCP-MCPDB (Fig. 1b(i)) includes the characteristic peaks at 2229 $cm^{-1}$, 1734 $cm^{-1}$, 1495 $cm^{-1}$, 1386 $cm^{-1}$, 1176 $cm^{-1}$, and 824 $cm^{-1}$ which correspond to the stretching bands of C≡N, C=O, $C_{aliphatic}$–O–$C_{aromatic}$, aromatic C=C, C–O, and the long aliphatic $CH_2$ of the spacer, respectively. The FT-IR spectrum of LCP-*b*-PDMAEMA (Fig. 1b(ii)) shows the same characteristic peaks of LCP-MCPDB with additional split peaks at 3404 $cm^{-1}$ and 3437 $cm^{-1}$, which correspond to the $NH_2$ stretching from PDMAEMA (inset). A shift in the C=O peak from 1710 $cm^{-1}$ to 1732 $cm^{-1}$ may be due to the intramolecular hydrogen bonding within PDMAEMA. Thus, successful block copolymerization using RAFT polymerization was confirmed by the FT-IR spectra of LCP-MCPDB and LCP-*b*-PDMAEMA.

### 3.2. Protein detection

Fig. 2a displays the polarized optical microscope images of the functionalized TEM grid cell with LCP-*b*-PDMAEMA ($TEM_{PDMAEMA}$ grid cell) under crossed polarizers after injecting solutions with and without protein at various pH values, ranging from 2 to 12. The images of the samples without proteins exhibit a change from the homeotropic to the planar orientation when the pH was between 6 and 7. PDMAEMA is a weak cationic polyelectrolyte with a pKa of 7.5; therefore, PDMAEMA is in the cationic and neutral states when the pH is below and above 7.5 as a result of protonation and deprotonation, respectively. The pH at which the H–P transition occurred (between 6 and 7) is slightly lower than the pKa of PDMAEMA (7.5). This discrepancy is likely due to the difference in the charge state of the brush relative to that of the bulk (freely moving polymer chain). However, the brightness of the polarized optical microscope images at pH 7 was lower than that of images at pH ≥ 8, which indicates that protonation of the PDMAEMA within the brush at pH 7 was minimal compared to that of the solutions at pH ≤ 6. Therefore, the pKa of PDMAEMA in the brush is likely reduced to between 6 and 7 from 7.5 in the bulk; however, additional systematic studies are necessary to determine the effect of the brush density on the protonation. Thus, the charged state of PDMAEMA generated the homeotropic orientation below its pKa threshold upon protonation, while the neutral state of PDMAEMA produced the planar orientation upon deprotonation. The charged state likely induced the electrical field at the LC/water interface to force the 5CB within the TEM grid to be oriented perpendicular to the LC/water interface because 5CB has a positive dielectric anisotropy and is capable of being oriented along an electrical field. The poly(acrylic acid)-b-poly(4-cyanobiphenyl-4′-oxyundecylacrylate) (PAA-*b*-LCP) functionalized TEM ($TEM_{PAA}$) grid cell described in our previous report [32] exhibited the homeotropic orientation when the pH was greater than the pKa due to the anionic charges of PAA. PAA is a weak anionic polyelectrolyte that exhibits a negative charge above (not below) its pKa as a result of deprotonation, such that the charged state of PAA occurs at high pH values. Thus, the charged state of weak polyelectrolytes (regardless of whether it is positive or negative) at the LC/water interface within the TEM grid cell is necessary to induce the homeotropic orientation as a result of an electric field being generated by polyelectrolytes located at the LC/water interface. A charged polyelectrolyte can form a complex with proteins through electrostatic interactions because proteins possess charges with their positive and negative portions existing below and above their pI's, respectively. For the cationic polyelectrolyte, the negatively charged proteins above the pI can form a complex. Therefore, complexes between proteins and the weak cationic polyelectrolyte can exist in the pH region between the pI of the protein and the pKa of the weak cationic polyelectrolyte. If the pI of the protein is higher than the pKa of the weak cationic polyelectrolyte, then it is impossible for the complex to form. BSA, Hb, and ChTg, which exhibit a pI of 4.7, 6.8, and 9.0, respectively, were tested in order to determine the required pH range for protein detection. The pKa value of PDMAEMA was determined to be between 6 and 7 from the data generated in the absence of protein, as previously mentioned, and only BSA has a pI below the pKa of PDMAEMA. Fig. 2b displays the polarized optical microscope images of the functionalized TEM grid cell containing LCP-*b*-PDMAEMA ($TEM_{PDMAEMA}$ grid cell) under the crossed polarizers after injecting BSA, Hb, or ChTg solutions (0.01 wt%, each above the critical concentration for the H–P transformation, which will be discussed in the following section) at pH values ranging from 2 to 12. After injecting the Hb and ChTg solutions, the polarized optical microscope images did not change much, which indicates that a complex did not form. However, when BSA was injected, the initial homeotropic orientation changed to the planar orientation when the pH was between 5 and 6, and the polarized optical microscope did not exhibit any noticeable changes at other pH values. The complexation between BSA and PDMAEMA is only possible between pH 5 and pH 6, which further confirms that the complex formed through electrostatic interactions can induce a change in orientation in 5CB within the TEM grid. To confirm the complexation between BSA and PDMAEMA, 0.1 wt% of BSA labeled with FITC ($BSA_{FITC}$) solution at pH 3, pH 6 and pH 9 was prepared and injected to the $TEM_{PDMAEMA}$ grid cell. Fig. 2ci–iii shows the fluorescent images of the $TEM_{PDMAEMA}$ grid cell after washing with a PBS buffer solution at the same pH. The green color was clearly observed on the TEM grid at pH 6, while black images were observed at pH 3 and pH 9, which indicates that the negatively charged $BSA_{FITC}$ formed electrostatic interactions with the oppositely charged polymer at pH 6 and no protein adsorption occurred at pH 3 and pH 9 due to the charges between the two species being the same. This result

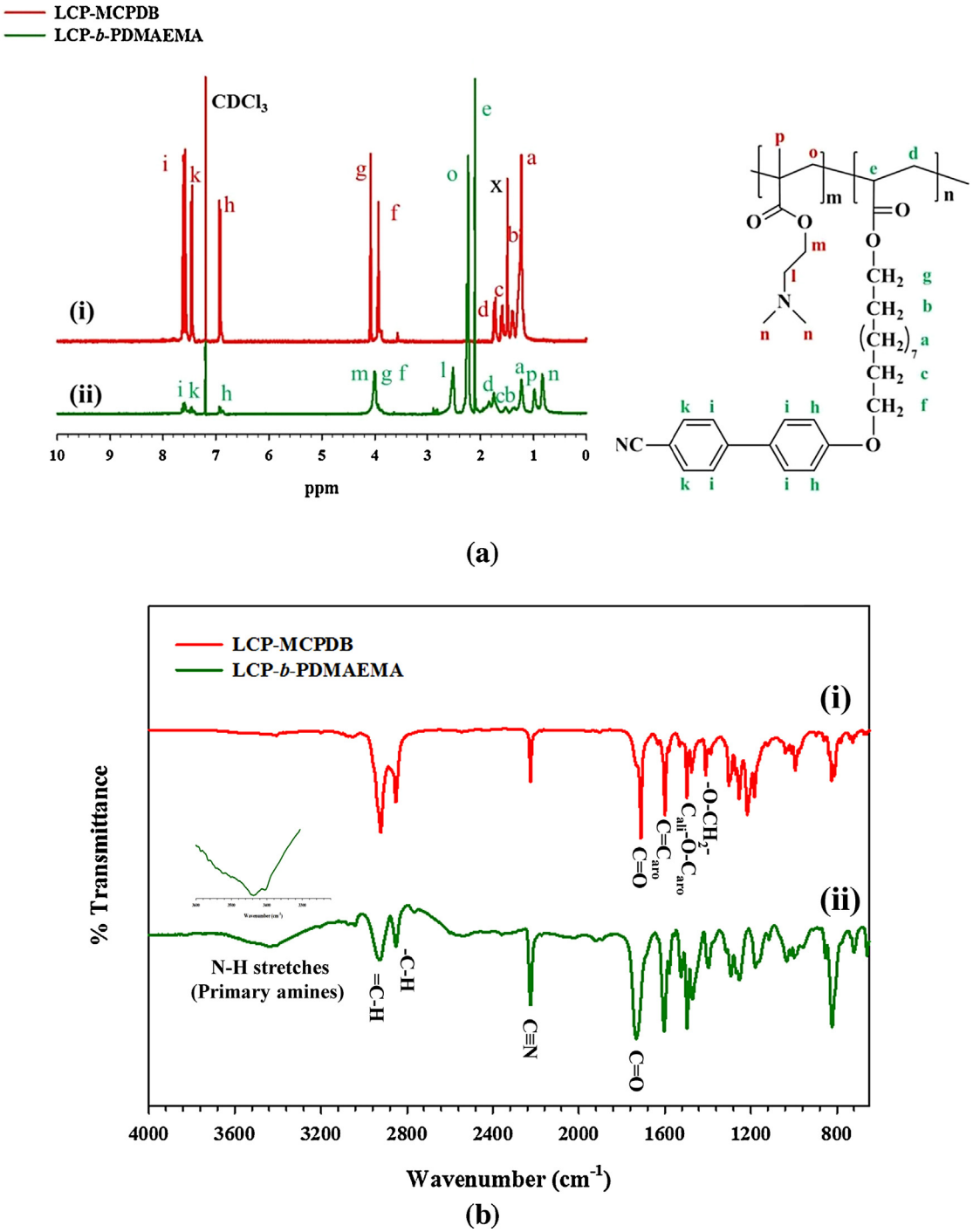


**Fig. 1.** (a) $^{1}$H NMR and (b) FT-IR spectra of (i) LCP-MCPDB and (ii) LCP-*b*-PDMAEMA.

confirms that the complex formed through electrostatic interactions can induce a change in orientation in 5CB within the TEM grid. This change in orientation occurs upon complex formation and is likely due to a decreased electrical field as a result of the neutrality of the complex, although further detailed studies on this mechanism are necessary.

Fig. 2b displays the polarized optical microscope images of the $TEM_{PDMAEMA}$ grid cell after injecting the BSA solution at pH 5 at protein concentrations ranging from 0.001 to 0.100 wt%. The pH of the tested protein solution was chosen to be above the pI in order to exhibit a negative net charge. The minimum protein detection limit through the H–P change was observed at 0.02 wt%, or 30 nM, for BSA. This low detection limit suggests that the weak cationic polyelectrolyte PDMAEMA could strongly bind to the protein via electrostatic interactions. The adsorption of proteins can occur in various ways including electrostatic interactions, hydrophobic interactions, and hydrogen bonding. These results suggest that electrostatic interactions are a major driving force for protein detection in polyelectrolyte LC-based biosensors.

Fig. SI 6a displays the polarized optical microscope image of the $TEM_{PDMAEMA}$ grid cells under crossed polarizers after injecting a BSA solution (0.02 wt%) at pH 6 into the cell. Fig. SI 6b displays

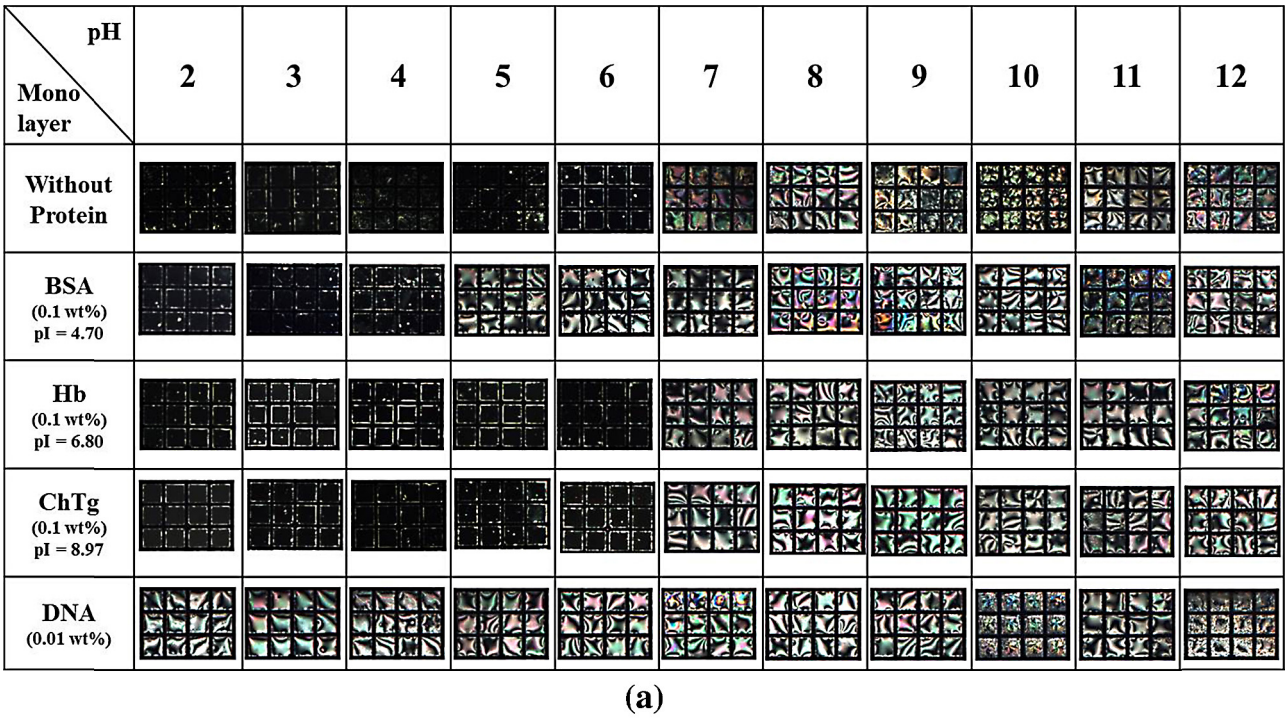


**Fig. 2.** (a) Polarized optical microscope images of the $TEM_{PDMAEMA}$ grid cell under cross polarizers without and with BSA, Hb, ChTg (all 0.1 wt%) and DNA (0.01 wt%) at various pH values ranging from 2 to 12, (b) samples containing BSA at various concentrations ranging from 0.001 to 0.100 wt% at pH 5 (the numbers in parentheses indicate concentration in μM), and (c) fluorescent images of the TEM grid cells after injecting a FITC-BSA (0.1 wt%) solution at (i) pH 3, (ii) pH 6, and (iii) pH 9.

the same image after replacing the pH 6 medium of the cell with a pH 3 aqueous buffer solution. Upon complexation between BSA and PDMAEMA, the initial planar orientation (Fig. SI 6a) did not change after washing with a pH 6 aqueous buffer solution without protein (data not shown), which suggests that the complexation was strong enough to be maintained after washing with water. The $TEM_{PDMAEMA}$ grid cell was then injected with a pH 3 aqueous solution that did not contain protein (Fig. SI 6c), which was performed by injecting 3 mL of the pH 3 aqueous buffer solution into the cell (volume, 0.6 mL). Changing the pH to 3 induced the positively charge state of PDMAEMA to occur and could potentially dismantle the complex between the BSA and PDMAEMA, resulting in the P-H change. However, the planar orientation did not change to the homeotropic state. There are several possible explanations for the irreversibility of the protein adsorption upon changing the pH above and below the pI. For example, the specific portion of charged protein that has already made contact with the PDMAEMA through electrostatic interactions could not be altered by changing

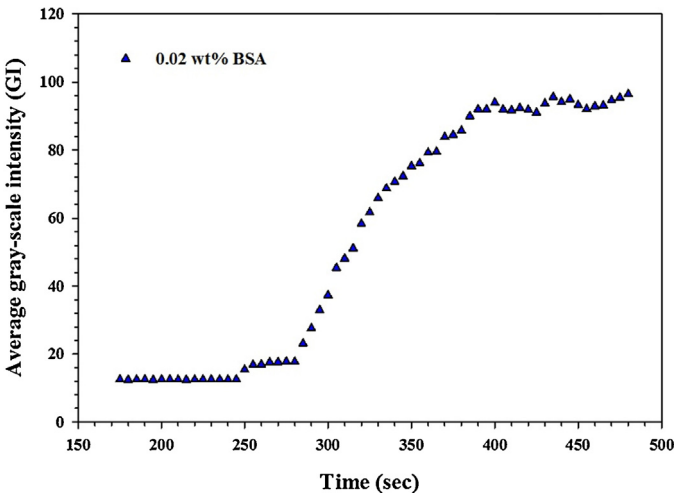


**Fig. 3.** Change in GI after injecting a BSA (0.02 wt%) solution into the TEM grid cell at pH 6.

the pH of the medium due to its strong binding force. Another possible explanation might be that the protein contained negatively charged groups even when the pH of the protein solution was lower than its pI, because the pI represents the relative amounts of negative and positive pendant groups, i.e., more positive groups than negative groups (as opposed to all positive groups) when the pH was lower than the pI.

### 3.3. Detection speed

Fig. 3 displays the change in the mean gray-scale intensity (GI) as a function of time after injecting the BSA solution (0.02 wt%) into the $TEM_{PDMAEMA}$ grid cell at pH 6. The concentration and the pH were chosen to be just above their detection limits (Fig. 2b) and pI, respectively. The GI gradually increased due to the H–P change in orientation upon the formation of a complex between the protein and PDMAEMA and eventually became saturated. The time for reaching the half-saturated intensity was 315 s after injecting the BSA. This time is slightly longer (by several seconds) than the times observed in our previous study with the $TEM_{PAA}$ cell [32]. This slow complexation within the $TEM_{PDMAEMA}$ grid cell is likely a result of the rapid change in the chain conformation of the PAA chains relative to the PDMAEMA chains.

### 3.4. DNA detection

As a strong anionic polyelectrolyte, DNA was soluble in the aqueous medium and was also negatively charged because of the phosphate deoxyribose backbone. The detection of salmon fish sperm DNA was tested with the $TEM_{PDMAEMA}$ grid cell. The pH dependency of DNA detection was also evaluated, as shown in Fig. 2a (last row). A strong anionic polyelectrolyte has negative charges regardless of pH and is capable of forming complexes with cationic PDMAEMA when the pH was lower than the pKa of PDMAEMA. The initial homeotropic orientation at $pH \leq 6$ changed to the planar orientation, which indicates that DNA formed a complex with PDMAEMA. However, the initial planar orientation at $pH \geq 7$ did not change upon the addition of DNA. Therefore, DNA could be detected in environments where the pH is below the pKa of PDMAEMA upon forming a complex with PDMAEMA (a weak polyelectrolyte) through electrostatic interactions. Fig. 4 displays the polarized optical microscope images of the $TEM_{PDMAEMA}$ grid cell after injecting DNA solutions at various concentrations ranging from 0.001 to 0.020 wt% within a pH 6 buffer solution. The initial homeotropic orientation changed to the planar orientation when the concentration was higher than 0.010 wt%. This detection limit for DNA (0.01 wt%) was lower than that observed for BSA (0.02 wt%) (Fig. 2b). This lower detection limit is likely a result of the stronger negative charge relative to the proteins because every nucleotide unit contains a negative phosphate deoxyribose group in DNA.

### 3.5. Stability

The stability of the $TEM_{PDMAEMA}$ grid cell can be tested by maintaining the reference homeotropic orientation. The homeotropic orientation in the $TEM_{PDMAEMA}$ grid cell cannot be maintained when the LCP-*b*-PDMAEMA or the 5CB is detached from the LC/water interface. Fig. 5 displays the mean GI of the $TEM_{PDMAEMA}$ grid cells at pH 3 as a function of time for a duration of 6 days. The homeotropic orientation produced a low GI value of 12 due to black image. The cell maintained its homeotropic orientation for 6 days, which indicates that the $TEM_{PDMAEMA}$ grid cell is quite stable during testing periods. The performance of the $TEM_{PDMAEMA}$ grid cell after 6

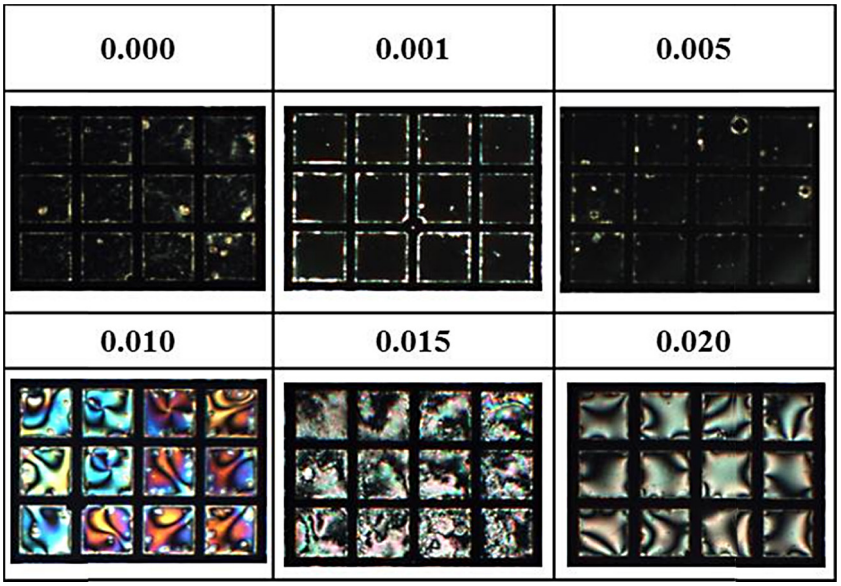


**Fig. 4.** Polarized optical microscope images of the TEM grid cells under crossed polarizers after injecting salmon fish sperm DNA at different concentrations. The number in the graph represents the wt% of the aqueous DNA solution at pH 6.

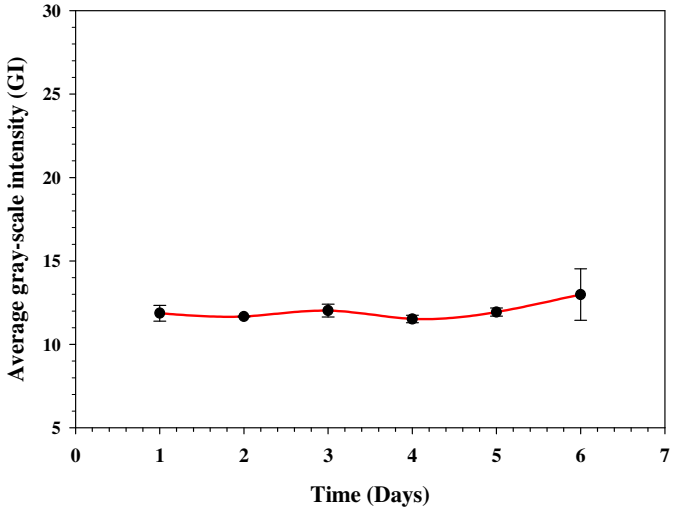


**Fig. 5.** The average GI of the $TEM_{PDMAEMA}$ grid cell as a function of time. The error bars represent the standard deviation for triplicate of experiments.

days was tested by injecting a BSA solution (0.02 wt%) into the cell. The cell converted to the planar orientation, which indicates that this $TEM_{PDMAEMA}$ grid cell was stable for a long time after the fabrication of the cell in water. This result is likely due to the strong anchoring of 5CB onto the grid by LCP-*b*-PDMAEMA.

## 4. Conclusions

In this report, we synthesized a weak polyelectrolyte containing LCP-*b*-PDMAEMA through RAFT polymerization to demonstrate its application as a biosensor for non-specific proteins and DNA. This system utilized a $TEM_{PDMAEMA}$ grid cell coated with a monolayer of LCP-*b*-PDMAEMA on the 5CB surface as a detecting layer by monitoring the H-P transformation. This functionalized TEM grid cell could detect proteins at a pH range above the pI of a protein and below pKa of PDMAEMA by electrostatic attractions within 1 min, with a detection limit of 30 nM for BSA. A strong anionic polyelectrolyte such as salmon fish sperm DNA could be detected with this $TEM_{PDMAEMA}$ grid cell at a wide pH range below the pKa of PDMAEMA with a detection limit of 0.01 wt% because it contains negatively charged phosphate deoxyribose groups throughout its structure regardless of the pH. This simple and inexpensive set-up for non-specific biomaterial detection provides the basic groundwork for developing effective and selective biosensors through the introduction of specific binding groups such as aptamers, antibodies, single-stranded DNA, proteins, peptides, and aptamer-binding RNA into the cell [37].

## Acknowledgements

This work was supported by the National Research Foundationof Korea (NRF-2011-0020264).

## Appendix A. Supplementary data

Supplementary data associated with this article can be found, in the online version, at http://dx.doi.org/10.1016/j.colsurfb.2014.06.028.

## References

[1] Y. Liu, T. Cui, Ion-sensitive field-effect transistor based pH sensors using nano self-assembled polyelectrolyte/nanoparticle multilayer films, Sens. Actuators B: Chem. 123 (2007) 148–152.
[2] M. Ozmen, E. Maltas, I.H. Patir, M. Bayrakci, Combined voltammetric and spectroscopic investigation of binding interaction between nifedipine and human serum albumin on polyelectrolyte modified ITO electrode, Electrochim. Acta 111 (2013) 535–542.
[3] Z. Wang, J. Yi, S. Yang, Direct electrochemistry and electrocatalysis of hemoglobin incorporated in composite film based on diblock weak polyelectrolyte PHAEMA-b-PDMAEMA and multi-walled carbon nanotubes, Sens. Actuators B: Chem. 176 (2013) 211–216.
[4] R. Zahn, J. Vörös, T. Zambelli, Swelling of electrochemically active polyelectrolyte multilayers, Curr. Opin. Colloid Interface Sci. 15 (2010) 427–434.
[5] K. Vermohlen, H. Lewandowski, H.D. Narres, M.J. Schwuger, Adsorption of polyelectrolytes onto oxides – the influence of ionic strength, molar mass, and $Ca^{2+}$ ions, Colloids Surfaces A – Physicochem. Eng. Asp. 163 (2000) 45–53.
[6] R. Greenwood, K. Kendall, Effect of ionic strength on the adsorption of cationic polyelectrolytes onto alumina studied using electroacoustic measurements, Powder Technol. 113 (2000) 148–157.
[7] P. Peng, G. Garnier, Effect of cationic polyacrylamide on precipitated calcium carbonate flocculation: kinetics, charge density and ionic strength, Colloids Surfaces A – Physicochem. Eng. Asp. 408 (2012) 32–39.
[8] N. Ali, W.-H. Sul, D.-Y. Lee, D.-H. Kim, S.-Y. Park, Structures of the cylindrical and vesicular micelles of an P4VP-longer asymmetric PS-b-P4VP, Macromol. Res. 17 (2009) 553–556.
[9] A. Pourjavadi, M.S. Amini-Fazl, H. Hosseinzadeh, Partially hydrolyzed crosslinked alginate-graft-polymethacrylamide as a novel biopolymer-based superabsorbent hydrogel having pH-responsive properties, Macromol. Res. 13 (2005) 45–53.
[10] L. Su, T. Shu, Z. Wang, J. Cheng, F. Xue, C. Li, X. Zhang, Immobilization of bovine serum albumin-protected gold nanoclusters by using polyelectrolytes of opposite charges for the development of the reusable fluorescent $Cu^{2+}$-sensor, Biosens. Bioelectron. 44 (2013) 16–20.
[11] Y. Li, H. Huang, Y. Li, X. Su, Highly sensitive fluorescent sensor for mercury (II) ion based on layer-by-layer self-assembled films fabricated with water-soluble fluorescent conjugated polymer, Sens. Actuators B: Chem. 188 (2013) 772–777.
[12] C. Ma, F. Zeng, G. Wu, S. Wu, A nanoparticle-supported fluorescence resonance energy transfer system formed via layer-by-layer approach as a ratiometric sensor for mercury ions in water, Anal. Chim. Acta 734 (2012) 69–78.
[13] M. Zhao, L. Yang, R. Zhang, J. Dong, H. Dong, Y. Wen, X. Zhan, G. Wang, Y. Lu, G. Wang, Detection of DNA hybridization by a pyrene-labeled polyelectrolyte prepared by ATRP, Polymer 54 (2013) 297–302.
[14] E.S. Read, S.P. Armes, Recent advances in shell cross-linked micelles, Chem. Commun. (2007) 3021–3035.
[15] V. Espina, E.C. Woodhouse, J. Wulfkuhle, H.D. Asmussen, E.F. Petricoin Iii, L.A. Liotta, Protein microarray detection strategies: focus on direct detection technologies, J. Immunol. Methods 290 (2004) 121–133.
[16] P.Y. Li, B. Lin, J. Gerstenmaier, B.T. Cunningham, A new method for label-free imaging of biomolecular interactions, Sens. Actuators B: Chem. 99 (2004) 6–13.
[17] A. Wittemann, M. Ballauff, Secondary structure analysis of proteins embedded in spherical polyelectrolyte brushes by FT-IR spectroscopy, Anal. Chem. 76 (2004) 2813–2819.
[18] M.Y. Shi Yunwei, Caiping Wang, Xianen Zhao, Rui Zhang, Jinma You, Determination of amino acids from hydrolyzed bovine serum albumin by high performance liquid chromatography and identification with electrospray ionization mass spectrometry, Chinese J. Anal. Chem. 34 (2006) 503–508.
[19] H. Wang, Y. He, X. He, W. Li, L. Chen, Y. Zhang, BSA-imprinted synthetic receptor for reversible template recognition, J. Sep. Sci. 32 (2009) 1981–1986.
[20] D.A. Winterbottom, R. Narayanaswamy, I.M. Raimundo Jr., Cholesteric liquid crystals for detection of organic vapours, Sens. Actuators B: Chem. 90 (2003) 52–57.
[21] X. Bi, S. Huang, D. Hartono, K.-L. Yang, Liquid-crystal based optical sensors for simultaneous detection of multiple glycine oligomers with micromolar concentrations, Sens. Actuators B: Chem. 127 (2007) 406–413.
[22] X. Bi, K.-L. Yang, Real-time liquid crystal-based glutaraldehyde sensor, Sens. Actuators B: Chem. 134 (2008) 432–437.
[23] V.K. Gupta, J.J. Skaife, T.B. Dubrovsky, N.L. Abbott, Optical amplification of ligand-receptor binding using liquid crystals, Science 279 (1998) 2077–2080.
[24] Y. Bai, N.L. Abbott, Enantiomeric interactions between liquid crystals and organized monolayers of tyrosine-containing dipeptides, J. Am. Chem. Soc. 134 (2012) 548–558.
[25] M.I. Kinsinger, B. Sun, N.L. Abbott, D.M. Lynn, Reversible control of ordering transitions at aqueous/liquid crystal interfaces using functional amphiphilic polymers, Adv. Mater. 19 (2007) 4208–4212.
[26] J.M. Brake, M.K. Daschner, Y.Y. Luk, N.L. Abbott, Biomolecular interactions at phospholipid-decorated surfaces of liquid crystals, Science 302 (2003) 2094–2097.
[27] J.M. Brake, A.D. Mezera, N.L. Abbott, Effect of surfactant structure on the orientation of liquid crystals at aqueous-liquid crystal interfaces, Langmuir 19 (2003) 6436–6442.
[28] N.A. Lockwood, N.L. Abbott, Self-assembly of surfactants and phospholipids at interfaces between aqueous phases and thermotropic liquid crystals, Curr. Opin. Colloid Interface Sci. 10 (2005) 111–120.
[29] M.I. Kinsinger, M.E. Buck, M.-V. Meli, N.L. Abbott, D.M. Lynn, Langmuir films of flexible polymers transferred to aqueous/liquid crystal interfaces induce uniform azimuthal alignment of the liquid crystal, J. Colloid Interface Sci. 341 (2010) 124–135.

[30] M. Khan, S.-Y. Park, Liquid crystal-based proton sensitive glucose biosensor, Anal. Chem. 86 (2013) 1493–1501.
[31] J. Kim, M. Khan, S.-Y. Park, Glucose sensor using liquid-crystal droplets made by microfluidics, ACS Appl. Mater. Interfaces 5 (2013) 13135–13139.
[32] J.M. Seo, W. Khan, S.Y. Park, Protein detection using aqueous/LC interfaces decorated with a novel polyacrylic acid block liquid crystalline polymer, Soft Matter 8 (2012) 198–203.
[33] D.-Y. Lee, J.-M. Seo, W. Khan, J.A. Kornfield, Z. Kurji, S.-Y. Park, pH-responsive aqueous/LC interfaces using SGLCP-b-polyacrylic acid block copolymers, Soft Matter 6 (2010) 1964–1970.
[34] S. Perrier, P. Takolpuckdee, J. Westwood, D.M. Lewis, Versatile chain transfer agents for reversible addition fragmentation chain transfer (RAFT) polymerization to synthesize functional polymeric architectures, Macromolecules 37 (2004) 2709–2717.
[35] W. Khan, J.M. Seo, S.Y. Park, Synthesis and micellization of a novel diblock copolymer of poly(N-isopropylacrylamide)-b-SGLCP and its application in stability of 5CB droplets in aqueous medium (vol 7, pg 780, 2011), Soft Matter 7 (2011), 11549-11549.
[36] J.C. Dubois, G. Decobert, P.L. Barny, S.C. Friedrich, C. Noel, Liquid crystalline side chain polymers derived from poly-acrylate, poly-methyacrylate and poly-α-chloroacrylate, Mol. Cryst. Liq. Cryst. 137 (1986) 349–364.
[37] D.Y. Lee, J.M. Seo, W. Khan, J.A. Kornfield, Z. Kurji, S.Y. Park, pH-responsive aqueous/LC interfaces using SGLCP-b-polyacrylic acid block copolymers, Soft Matter 6 (2010) 1964–1970.